

UPCommons

Portal del coneixement obert de la UPC

<http://upcommons.upc.edu/e-prints>

Aquesta és una còpia de la versió *author's final draft* d'un article publicat a la revista Polymer Degradation and Stability.

URL d'aquest document a UPCommons E-prints:
<http://hdl.handle.net/2117/121885>

Article publicat / *Published paper:*

Realinho, V., Haurie, L., Formosa, J., Velasco, J.I. (2018) Flame retardancy effect of combined ammonium polyphosphate and aluminium diethyl phosphinate in acrylonitrile-butadiene-styrene. Polymer Degradation and Stability, vol. 155, p. 208-219. Doi: 10.1016/j.polymdegradstab.2018.07.022

Flame retardancy effect of combined ammonium polyphosphate and aluminium diethyl phosphinate in acrylonitrile-butadiene-styrene

Vera Realinho^{a*}, Laia Haurie^b, Joan Formosa^c, José Ignacio Velasco^a

^a Centre Català del Plàstic, Departament de Ciència dels Materials i Enginyeria Metal·lúrgica, Universitat Politècnica de Catalunya-Barcelona Tech, C/ Colom 114, E-08222 Terrassa, Barcelona, Spain

^b Department de Tecnologia de l'Arquitectura, Universitat Politècnica de Catalunya, Av. Dr. Marañon 44-50, E-08028 Barcelona, Spain

^c Departament de Ciència dels Materials i Química Física, Facultat de Química, Universitat de Barcelona, Martí i Franquès, 1, E-08028 Barcelona, Spain

* Corresponding author: vera.realinho@upc.edu

Abstract

The present work investigates the fire retardancy mechanism of ammonium polyphosphate (APP) and aluminium di-ethyl phosphinate salt (AlPi) in an acrylonitrile-butadiene-styrene copolymer (ABS) by analysing the pyrolysis, flammability and fire behaviour. Evidences of synergy in flammability by combining both flame retardants were discussed and related to flame retardant mechanisms assessed by means of TGA and FT-IR analysis of the pyrolysis gases. Specifically, the ABS flame retardant formulation with a 12.5 wt% APP and 12.5 wt% AlPi (ABS-APP/AlPi) reached a UL-94 V-0 classification, unlike the ABS with 25 wt% APP (ABS-APP) and ABS with 25wt% AlPi (ABS-AlPi) formulations, which completely burned. Under forced flame conditions, APP and AlPi showed, respectively, a main condensed and gas phase-based mode of action in the ABS matrix, whereas, a combined gas and condensed mode of action was identified when both additives were simultaneously incorporated. Also, the ABS-APP/AlPi formulation showed the higher reduction of the peak heat release rate (74 %) and of the maximum average rate of heat emission (65 %), obtained from cone calorimeter tests. As well as, a protective fire residue with an improved microstructure assed by SEM.

Keywords: ABS, phosphorous flame retardants, flame retardancy.

1. Introduction

Acrylonitrile-butadiene-styrene (ABS) due to its high toughness and impact strength, chemical resistance advantages and good processability is commonly used as an engineering thermoplastic for several industrial and domestic appliances. However, one of the main drawbacks of ABS is its inherent flammability and dripping, which could limit its applications [1, 2]. Environmental considerations have given way for the increased use of phosphorus-based flame retardants (PFR) as alternatives to the halogen-containing compounds [3], traditionally used as flame retardants for ABS [4-7], and in the past decades, high melt temperature and soluble PFR have been used [8-11]. They exhibit all kinds of flame retardant modes of action, such as flame inhibition in the gas phase, char enhancement, and intumescence and formation of inorganic glass in the condensed phase [12].

It has been found that PFR effectiveness depends of the polymer matrix [13, 14]. Polymers with oxygen and/or nitrogen on their structure interact more favorably with these additives, leading to an improvement of the fire behavior [15]. Kim, et. al [16], found that such effectiveness strongly depends on the P content and that a 5 wt% P is required to observe an exhibit self-extinguishing behavior in ABS. Moreover, Rabe et al. [12] found the existence of a critical content of PFR, from which the level of degradation changes significantly up to the retention of incompletely pyrolyzed polymer due to a protective layer.

Several works have been published related with the flame retardant efficiency of ammonium polyphosphate (APP) on non-charring and self-charring polymers [17-20], where it has been proved that APP has a major role in the condensed phase [15]. The efficiency and mechanism of action of diethyl aluminium phosphinate (AlPi) have been less studied, and it has been found to be dependent of the polymer matrix [16]. Sullalti et al. [21] reported that AlPi acted mainly in the condensed phase, forming a consistent amount of char in PBT. Braun et al. [22] reported that AlPi had a higher effect in the gas phase in PA6,6 through the release of diethylphosphic acid, providing flame inhibition. Similar effects were observed in a thermoplastic elastomer-based multisystem [14]. Hence, the flame retardant efficiency and mechanism of AlPi associated with the polymer characteristic need to be further studied.

In the present paper a preliminary study about the effects of combining an ammonium polyphosphate (APP) and a di-ethyl aluminium phosphinate (AlPi) in ABS

matrix is carried-out, by analysing eventual synergistic effects and/or interferences on their individual mode of action.

2. Experimental

2.1. Materials and compounding

An acrylonitrile-butadiene-styrene copolymer (ABS), with the commercial name of *ELIXTM 128 IG*, was provided by *Elix Polymers* (Tarragona, Spain) in the form of pellets. According to the manufacturer information, ABS contains 26-28 wt% of butadiene and has a melt volume flow rate of 15 cm³/10 min, measured at 220°C and 10 kg. Two phosphorus flame retardant (PFR) additives were used: an ammonium polyphosphate (APP), *Exolit® AP422*, and an aluminium diethylphosphinate (AlPi), *Exolit® OPI230*, both kindly supplied, in form of white powder by *Clariant Produkte (Sulzbach, Deutschland)*. The APP, with chemical formula of (NH₄PO₃)_n, possess a polymerization grade (n) higher than 1000 and a phosphorus and nitrogen content of 31-32 wt% and 14-15 wt% respectively; a density of 1.90 g/cm³ and an average particle size of 15 µm. The AlPi, with chemical formula of [(C₂H₅)₂PO₂]₃Al, has a phosphorus content of 23.3-24 wt%, a density of 1.35 g/cm³ and an average particle size of 30 µm, as reported by the manufacturer.

The ABS was dried at 80 °C during 4 hours and the PFR additives at 100 °C overnight previous to melt compounding. Three formulations were prepared with 25 wt% APP, AlPi and APP/AlPi in a 1:1 mass proportion (see table 1). The weight percentage of APP/AlPi was established based on information provided by the supplier and on typical values used in phosphorus flame retardants formulations [23]. The ABS-APP or ABS-AlPi formulations were used to ascertain the APP and AlPi individual mechanism of action and help to discern the interactions between both of them and the polymer matrix.

Table 1: Composition of ABS flame retardant formulations.

| Material code | ABS (wt%) | APP (wt%) | AlPi (%) |
|---------------|-----------|-----------|----------|
| ABS | 100 | - | - |
| ABS-APP | 75 | 25 | - |
| ABS-AlPi | 75 | - | 25 |
| ABS-APP/AlPi | 75 | 12.5 | 12.5 |

The blending temperature was 160 °C in a *Brabender* mixing chamber, with a rotating rate of 30-60 rpm applied for 15 min. Pure ABS was also melt-mixed under the same conditions for comparison. Afterwards, the compounds were placed into a mould of 150 x 150 and 4 mm³, in order to prepare plates by compression moulding from which specimens were cut for later testing and characterization. A hot-plate press (*IQAP-LAP PL-15*) was used, applying a temperature of 165°C for 15 min, 2 min of which under 90 bar of pressure. Subsequent cooling, under a constant pressure of 90 bar, was applied at the end of the compression cycle.

2.2. Characterization procedure

The thermal stability of the samples was evaluated by means of thermogravimetric analysis (TGA). TGA was performed in nitrogen atmosphere using a SDT Q600 equipment (TA Instruments, UK) with a constant heating rate of 10 °C min⁻¹ from 40 to 1000 °C. For each experiment a mass of 20 mg ± 0.5 mg and a gas flow rate of 100 mL min⁻¹ were used. TGA coupled with IR was performed in order to characterize the volatile emissions during the decomposition of the samples under study by means of a TG-IR-GCMS Interface TL8000 (Perkin Elmer, USA) and a IR Spectrum Two™ equipment (Perkin Elmer, USA). The interface device operated at a gas flow of 80 mL·min⁻¹ and a temperature of 250 °C.

The flammability behaviour was investigated by the UL-94 test on 127x12.7x4 mm³ specimens ignited from bottom in the vertical configuration according to the standard of UL-94 (Underwriters Laboratories, USA). The best flame retarded performance was classified to be V0 when burning time was short (the sum of the two ignitions lower than 50 s) and no dripping of flaming particles was present. The worst was named “not classified” (NC) and corresponded to specimens burned completely. Limiting oxygen index (LOI) measurements were performed in an oxygen/nitrogen atmosphere, in accordance with ISO 4589 standard, on 80x10x4 mm³ specimens.

Cone calorimeter tests were carried out by means of a cone calorimeter (Ineltec, Spain). Test specimens with a diameter of 72 ± 2 mm and thickness of 4 ± 0.5 mm, were irradiated with a constant heat flux of 35 kW/m² at a constant distance of 25 mm. Reaction-to-fire parameters such as time to ignition (TTI), peak of the heat release rate (PHRR), maximum average rate of heat emission (MARHE), total heat emitted (THE) and effective heat of combustion (EHC) were determined from curves of heat release rate (HRR) versus time. Moreover, the residue microstructure of the samples after the

cone calorimeter tests was analysed by means of scanning electron microscopy (SEM) using a JEOL JSM-5610 microscope. The samples were sputtered with a thin layer of gold before the analysis.

3. Results and discussion

3.1. Thermal stability

The thermal stability of individual PFR additives was firstly analysed by TGA. The data, including the temperature corresponding to the maximum mass loss rate (T_{peak}), mass loss rate (MLR) and mass loss (ML) of each thermal decomposition (TD) stage, as well as the total fraction of residue (R) remaining at 700 and 1000 °C, are collected in Table 2.

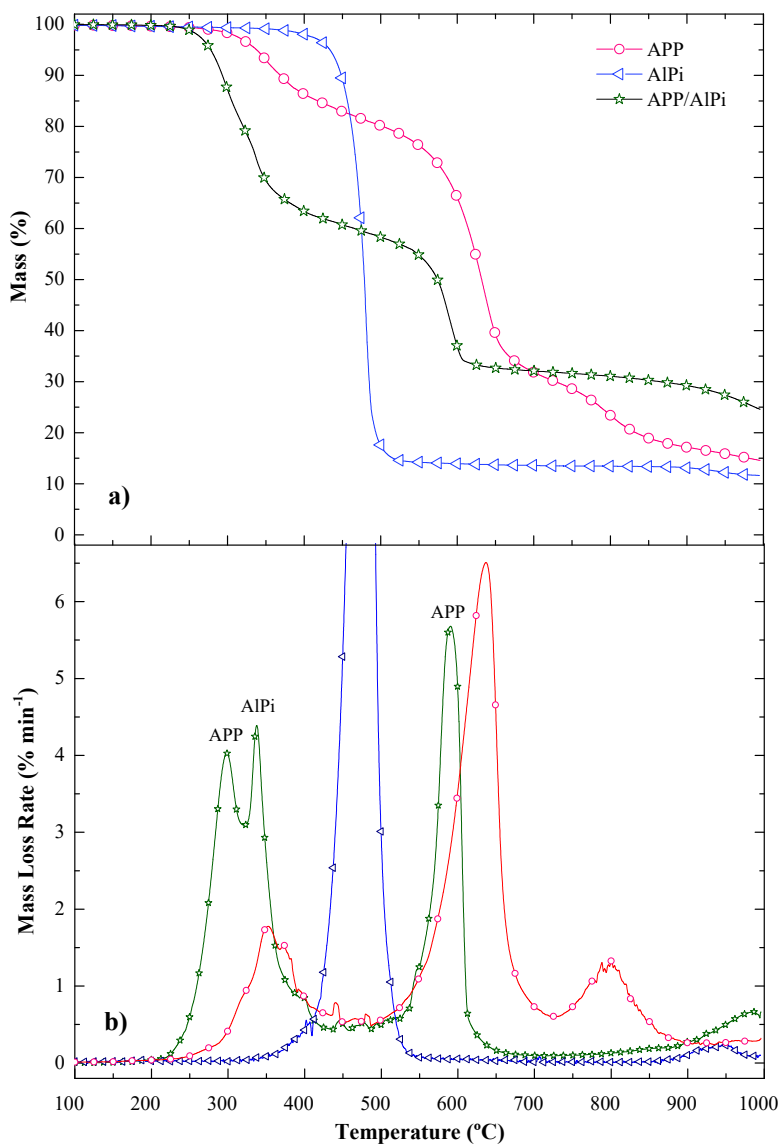


Figure 1: TG a) and dTG b) curves of APP, AlPi and APP/AlPi obtained at 10°C/min under N₂.

APP thermally decomposed in three steps (Figure 1). The first step occurred, approximately, between 250 °C and 450 °C, with a mass loss of 18.7% and a maximum of mass loss rate at 350 °C. In this step, according to literature, APP decomposed releasing ammonia and polyphosphoric acid, which undergone simultaneously a transformation into vitreous crosslinked ultraphosphate with release of water [24, 25]. The second mass loss step occurred between 480 °C and 710 °C, with a mass loss of 50.8% and a maximum of mass loss rate at 637 °C. In this stage, the crosslinked vitreous ultraphosphate fragmented to form volatile phosphorus oxide [24], which provides to APP a flame retardant effect in the gas phase. The third and last step, with a mass loss of 13.3 %, occurred approximately between 710 °C and 900 °C and proposed to be due to the decomposition of a higher thermally stable fraction of crosslinked phosphates or due to further decomposition of the substrate thermally isolated by the vitreous ultraphosphate layer.

Table 2: TG and dTG data of thermal degradation and residue of PFR additives.

| PFR | TD stage | Temperature range (°C) | T _{peak} (°C) | MLR (% min ⁻¹) | ML (%) | R _{700 °C} (%) | R _{1000 °C} (%) |
|----------|----------|------------------------|------------------------|----------------------------|--------|-------------------------|--------------------------|
| APP | 1 | 250-450 | 350 | 0.18 | 18.7 | 31.8 | 14.6 |
| | 2 | 480-710 | 637 | 6.50 | 50.8 | | |
| | 3 | 710-900 | 787 | 0.14 | 13.3 | | |
| AlPi | 1 | 340-550 | 481 | 38.0 | 86.0 | 13.6 | 11.6 |
| | 2 | 850-1000 | 954 | 0.24 | 1.8 | | |
| APP/AlPi | 1 | 220-480 | 298/337 | 4.1/4.7 | 40.4 | 32.1 | 24.6 |
| | 2 | 480-680 | 588 | 5.7 | 27.0 | | |
| | 3 | 780-1000 | 995 | 0.66 | 6.7 | | |

The AlPi, decomposed in two stages. The first and major one, between 340 °C and 550 °C, has a mass loss of 86 % with a temperature of the maximum mass loss at 481 °C. The second stage, with a less significant mass loss (1.8%) was registered at higher temperature, between 850 °C and 1000 °C. It has been discussed that AlPi partly vaporises and partly decomposes to diethylphosphinic acid and ethane, with aluminium phosphates remained in the residue [22, 26, 27].

The mixture of APP and AlPi, with a mass ratio of 1:1, showed different degradation pattern by lowering the degradation temperature with the overlapping of the first degradations steps of both additives. A more thermally stable residue was formed at lower temperature than that of APP. Indeed, the APP/AlPi system present higher

residual mass than that the sum of APP and AlPi contribution at 700°C or 1000 °C (41% and 88% higher respectively). This means that, between APP and AlP, strong interactions were taken place that led to an enhancement of the condensed phase mechanism of action.

The evolution of the mass loss with temperature (TG) and respective derivative curves (dTG curves) of ABS and ABS flame retardant systems are displayed in Figure 2 and the related data are summarized in Table 3.

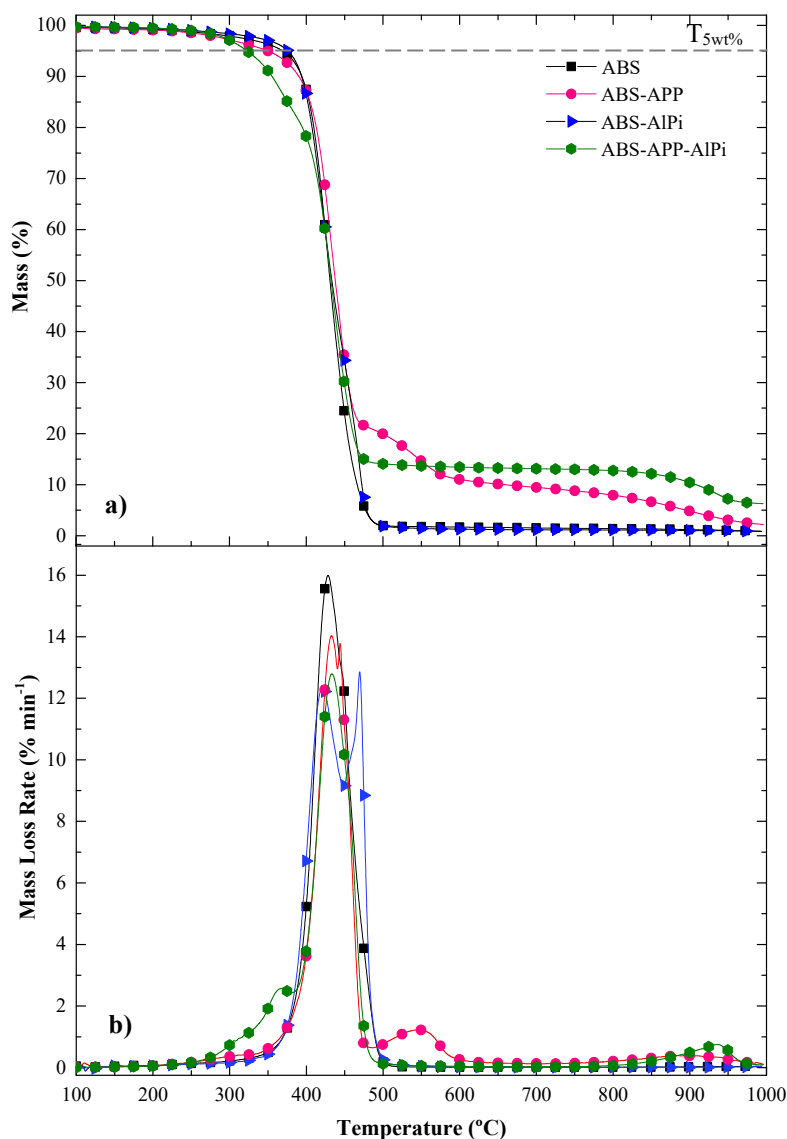


Figure 2: TG a) and dTG curves b) of ABS and its flame retardant containing samples, obtained at 10°C/min under nitrogen atmosphere.

ABS exhibit a one-stage degradation process, between 230 and 525°C with 5% ($T_{5\%}$) and maximum mass loss rate (T_{peak}) occurring at 369 °C and 427 °C, respectively.

Also, the polymer did not show a significant residue formation, which demonstrate that it has no ability of charring by itself. A similar behavior was observed in the presence of AlPi, with no residue formation even at 500°C. Although, this additive by itself showed residue formation (see Figure 1), in ABS and at a content of 25 wt%, it completely volatilized within a slightly higher range of temperature than ABS thermal decomposition. Additionally, in Figure 2 b), it is possible to see a doublet at 421°C and 470 °C that was attributed to the ABS and AlPi maximum mass loss decomposition, respectively. So, based on these results, AlPi was more thermally stable than ABS and a not efficient charring agent. Contrary to ABS-AlPi, the ABS-APP and ABS-APP/AlPi showed a T_{5%} decrease of 19 °C and 46 °C, respectively, as well as, a slight increase of the T_{peak} regarding the neat ABS. Indeed, the presence of both additives promote a higher actuation on the gas phase, with a 15.1% of mass loss between 230 °C and 380 °C and with the maximum mass loss occurring at 370 °C. The presence of APP in ABS promoted a higher char formation above 450 °C, being the residue more thermally stable in the ABS-APP/AlPi system, when both additives were added. In fact, ABS-APP/AlPi presented a higher residue content at 700 °C and 1000 °C than ABS-APP (Table 3), starting its last decomposition step approximately 100 °C above the ABS-APP formulation.

Table 3: TG and dTG data of thermal degradation and residue of ABS and ABS formulations.

| Materials | TD step | Temperature range (°C) | T _{peak} (°C) | MLR (% min ⁻¹) | ML (%) | R _{700 °C} (%) | R _{1000 °C} (%) |
|--------------|---------|------------------------|------------------------|----------------------------|--------|-------------------------|--------------------------|
| ABS | 1 | 230-525 | 427 | 16.1 | 97.1 | 1.5 | 1.2 |
| ABS-APP | 1 | 230-485 | 433 | 14.1 | 78.0 | 9.5 | 2.2 |
| | 2 | 485-680 | 544 | 1.23 | 11.2 | | |
| | 3 | 680-1000 | 895 | 0.39 | 7.5 | | |
| ABS-AlPi | 1 | 250-450 | 421 | 12.4 | 65.0 | 1.2 | 1.1 |
| | 2 | 450-570 | 470 | 13.2 | 32.7 | | |
| ABS-APP/AlPi | 1 | 230-380 | 370 | 2.58 | 15.1 | 13.2 | 6.3 |
| | 2 | 380-550 | 432 | 12.9 | 70.2 | | |
| | 3 | 780-1000 | 935 | 0.75 | 6.6 | | |

To further investigate the synergistic effects between APP and AlPi in the ABS-APP/AlPi formulation, a comparative between the calculated and experimental TG curves was made (see Figure 3). The calculated curve was determined based upon the weight percentage of the components in the material. It was found that, between 230 °C

and 350 °C, the degradation accelerated more than expected. Based on this fact, an enhancement of the gas phase mechanism of action promoted by the presence of these two phosphorous additives in ABS occurred. Furthermore, when the temperature was higher than approximately 525 °C, the experimental residue surpassed the theoretical one. This reinforces the evidence of synergistic effects between those additives, that led to the formation of a more thermally stable residue than expected. Contributed, by this way, to a more efficient action on the condensed phase when combined, as mentioned before.

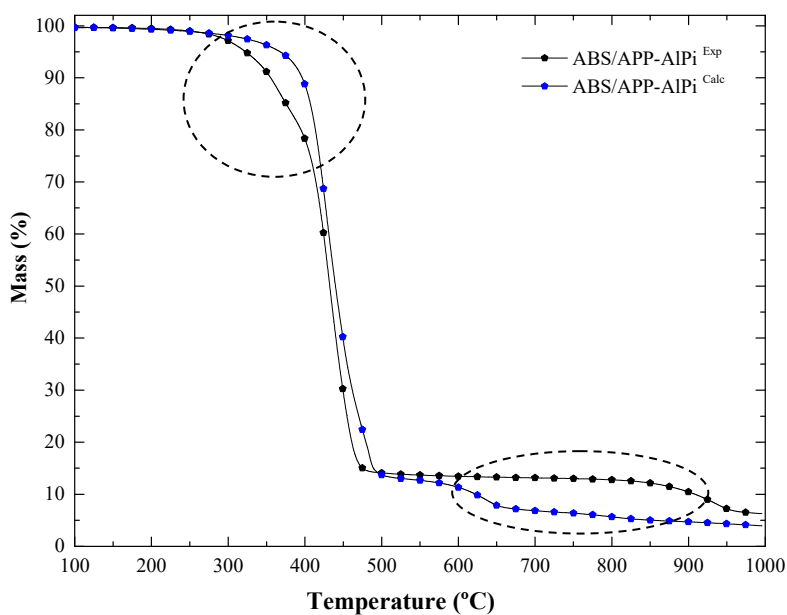


Figure 3: Experimental and calculated TG curves of ABS-APP/AlPi system.

3.2. FTIR Spectra of the Gas Phase

The FTIR characteristic spectra of the gaseous pyrolysis products, obtained at the T_{peak} of the main steps decomposition, of APP, AlPi and APP/AlPi are presented in Figure 4. During the APP's decomposition first step, two sharp absorbance peaks were registered at 930 cm^{-1} and 960 cm^{-1} and attributed to ammonia gas (NH_3) absorptions, with its maximum absorbance registered at 350 °C (Figure 4 a)). The absorbance peak registered at 1627 cm^{-1} was assigned to the NH_3 asymmetric bend vibration [28]. It should be mentioned that the numerous thin peaks around 3335 cm^{-1} and those between 750 and 1250 cm^{-1} are also characteristics of the release of NH_3 ; and the peaks lying between 3500 - 3800 cm^{-1} and 1400 - 1700 cm^{-1} are attributed to the release of water (H_2O) [29]. This illustrates well the decomposition of APP mentioned previously and is in accordance with the literature [30]. Regarding to APP's second step, a new broad band between 3400 cm^{-1} and 2400 cm^{-1} was registered and assigned to P-OH absorption [22],

as well as, characteristics signs at 1285 and 1090 cm^{-1} of P=O and P-O, and related to the release to the stretching vibration of volatile phosphorus radicals.

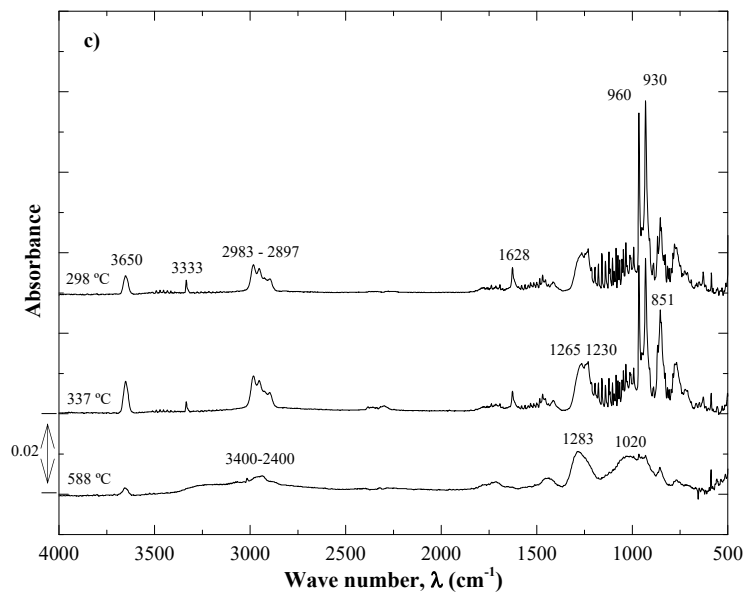
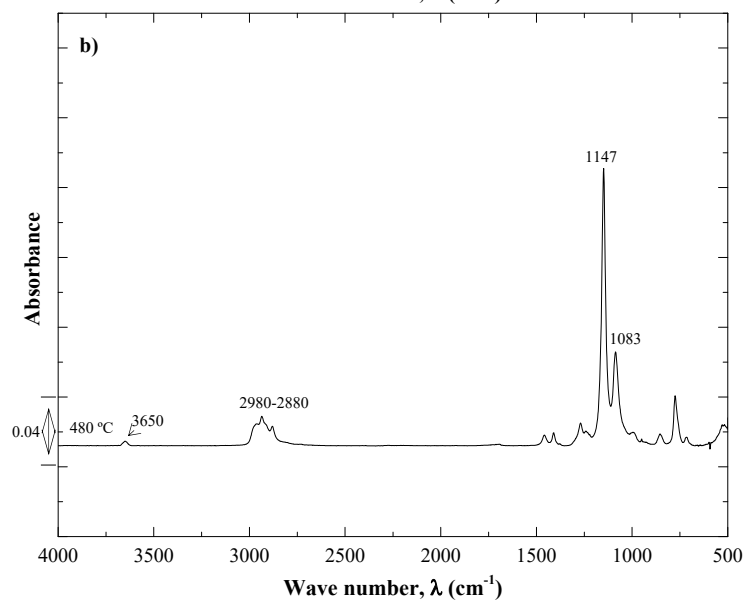
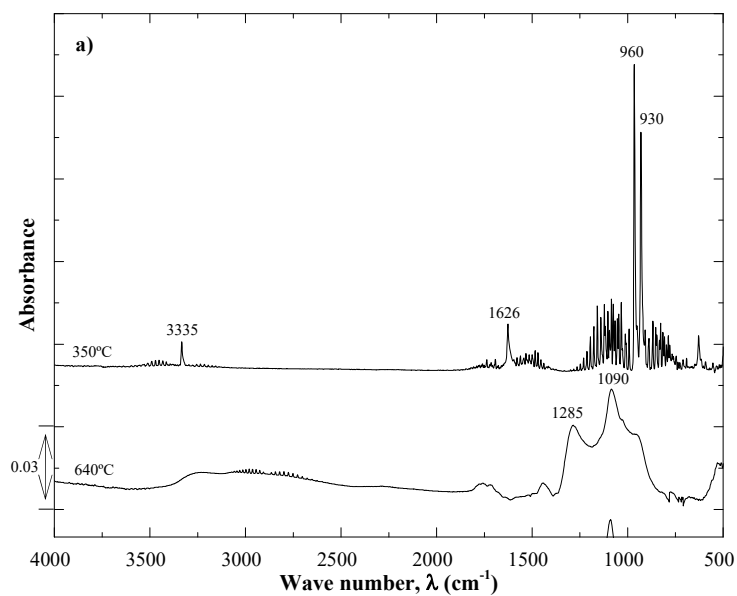


Figure 4: FT-IR spectra of a) APP, b) AlPi and c) APP/AlPi pyrolysis products at the temperature of maximum mass loss rate.

The aluminium diethylphosphinate $[(C_2H_5)_2PO_2]_3$, compared with ammonium polyphosphate generates a higher amount of volatile compounds in a limited range of temperature (between 340-550 °C, see table 3). It has been reported that AlPi undergoes thermal decomposition to yield ethylene (C_2H_2) and diethylphosphinic acid. The last one generates phosphorus radicals such PO, PO_2 , HOPO and $HOPO_2$, that inhibit the combustion process in the gas phase by acting like reactive sites to recombine $\cdot H$ and $\cdot OH$ radicals in order to form less combustible or more stable compounds or radicals [31]. The characteristics signals of P-O (1147 and 1083 cm^{-1}) and P-OH stretch (3650 cm^{-1}) can be seen in Figure 4 b). The hydrocarbon signs of ethylene were also registered between 2980 and 2880 cm^{-1} .

It is generally agreed that APP, a precursor of polyphosphoric acid, is capable of affecting the thermal stability of other components, because it promotes acid hydrolytic reaction of the substrates [30]. So, it is assumed that AlPi hydrolytic decomposes at lower temperature to produce diethylphosphinic acid and aluminium trihydroxide, which further thermal decompose to produce phosphinate volatiles and water, respectively. As is possible to see in Figure 4 c), the vibration signals at 1280-1220 and 870-820 cm^{-1} (stretching and bending vibrations of P=O), appeared at the same temperature range of APP's first decomposition step. These signals, and that registered at 3650 cm^{-1} , are indicative of the synergistic effects of both PFR by the formations of active free radical-quenching capability (phosphorus radicals), demonstrating that free radicals like $\cdot H$ and $\cdot OH$ could be quenched and the flame could be suppressed simultaneously [32] at a range of temperature that could interfere on ABS decomposition.

FT-IR spectrum of ABS (Figure 5 a)), showed the typical aromatic and aliphatic hydrocarbon vibrations at 3032 cm^{-1} , 3072 cm^{-1} and 2873 cm^{-1} , 2937 cm^{-1} respectively. Additionally, the deformation of CH_2 of butadiene at 1492 and 1450 cm^{-1} and out-of-plane vibration of C=C-H in butadiene at 910 cm^{-1} [33] can be noted. These hydrocarbons are mainly consequences of the chain scission of the polymer to give out monomers [28]. From FT-IR spectra of ABS, registered at different temperature, (Figure 5 b)) it was noted that decomposition at butadiene region started a little earlier

and it lasted slightly longer than the styrene part, which is consistent with results previously found [28, 34].

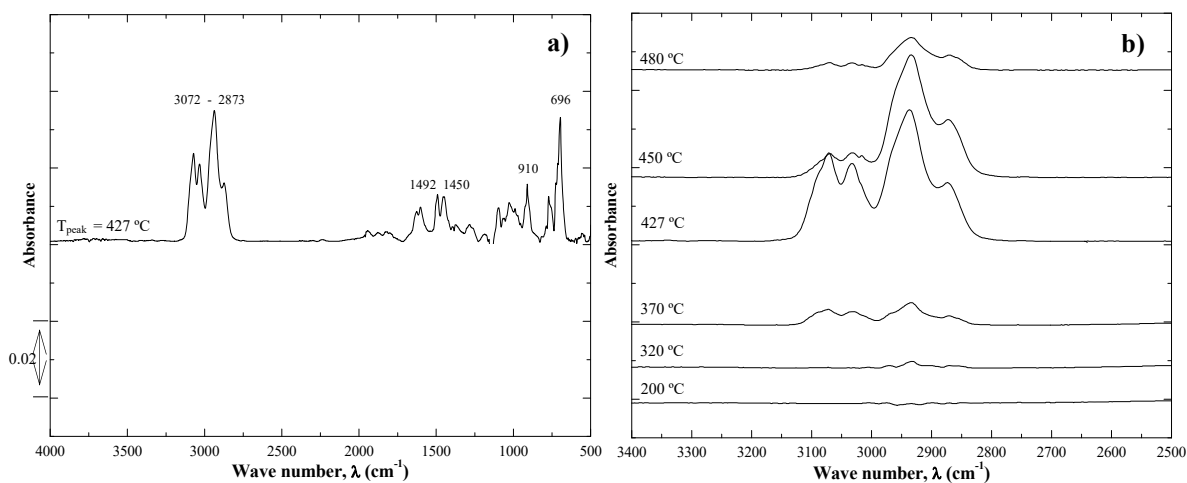


Figure 5: FTIR spectra of ABS pyrolysis gases obtained at a) the temperature of maximum mass loss rate and at b) different temperature between 3400 cm^{-1} and 2500 cm^{-1} of wavenumber.

Figure 6 shows the ABS-APP FT-IR pyrolysis gases spectra obtained at the beginning of decomposition and at the temperature of the maximum mass loss rate of each step decomposition. ABS-APP formulation loosed almost the 80% of its weight during its first step decomposition (between 230 °C and 485 °C). This step was attributed mainly to decomposition of ABS and to partial APP decomposition. APP started to decompose at a slightly lower temperature than ABS, with the release of ammonia and water as discussed before. Furthermore, ammonia evolution from APP is related to acidic site formation in the intumescent phenomena as already reported in the literature [35, 36]. So, at this range of temperature it is expected the formation of a carbonaceous layer on the condensed phase. At the second step of ABS-APP decomposition, the amount of pyrolysis gases was lower regarding to the first one. Two small broad peaks were registered at 1260 cm^{-1} and 1090 cm^{-1} associated to the stretching of P=O and P-O, respectively [37, 22, 38]. These have been related with volatile phosphorus oxide release by the fragmentation of the cross-linked ultraphosphates [30].

FT-IR spectra of ABS-ALPi pyrolysis gases are shown in Figure 7. ABS started to decompose first than ALPi, since that only characteristics absorption peaks of the ABS aromatic and hydrocarbon vibrations were observed at 390 °C. Nevertheless, at the first step T_{peak} (421 °C) a small absorbance peak at 1150 cm^{-1} was also noted, indicating the presence of a fraction of phosphorus radicals.

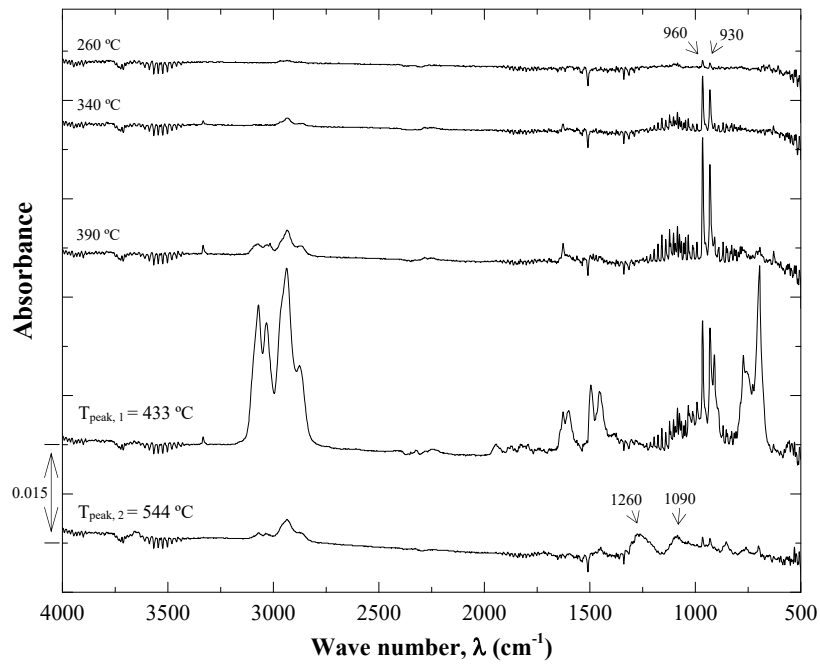


Figure 6: FT-IR spectra of ABS-APP pyrolysis products at the temperature of the maximum mass loss rate and at the beginning of decomposition.

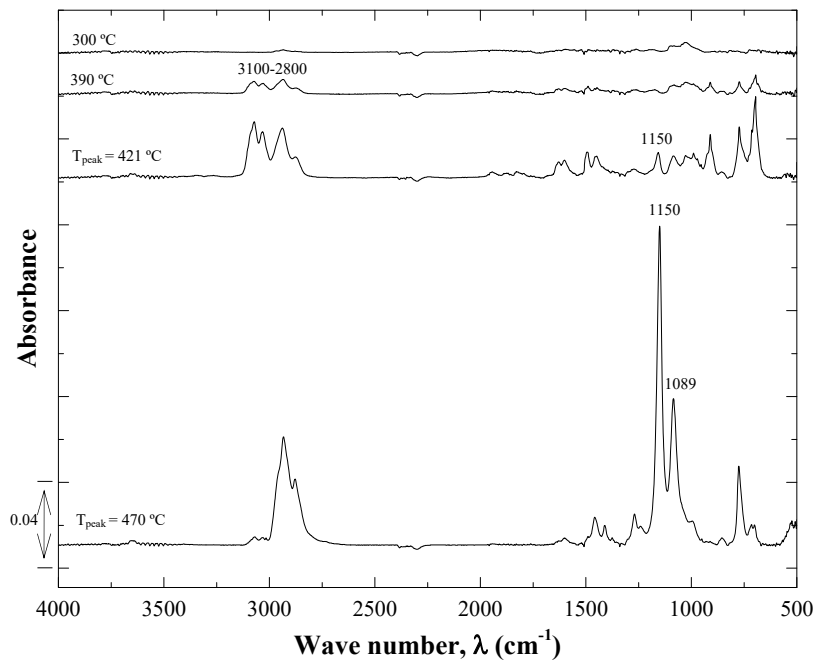


Figure 7: FT-IR spectra of ABS-APi pyrolysis products at the temperature of the maximum mass loss rate and at the beginning of decomposition.

Finally, from Figure 8, it was possible to see that ABS-APP/AlPi started to decompose at a similar temperature than ABS-APP. In this formulation, at 260 °C, very small absorbance sign (3100-2800 cm^{-1}) attributed to the ABS hydrocarbons vibration and the typical absorption peaks of ammonia (960 and 930 cm^{-1}) were observed. Moreover, new signs attributed to P=O stretching, bending and symmetric stretch vibrations (1280-1220 cm^{-1} , 870-820 cm^{-1} and 770 cm^{-1} , respectively) were registered. As well as, an absorbance peak at 3650 cm^{-1} related to P-OH stretching vibrations, indicating the release of phosphorus radicals during ABS step decomposition. As pyrolysis proceed, both aromatic and hydrocarbons typical absorbance from ABS were noted. The signs observed in ABS-AlPi (1150 cm^{-1} and 1089 cm^{-1}) did not appeared in this case, which state that AlPi did not completely volatilized, indicating that part of the phosphorus remained in the residue. So, this residue was more thermally stable than that of ABS-APP, because its decomposition occurred at much higher temperature (T_{peak} of 935 °C). Also, the APP/AlPi degradation step observed at a T_{peak} of 588 °C was not registered for ABS-APP/AlPi, which supports the strong interactions between the PFR and the ABS.

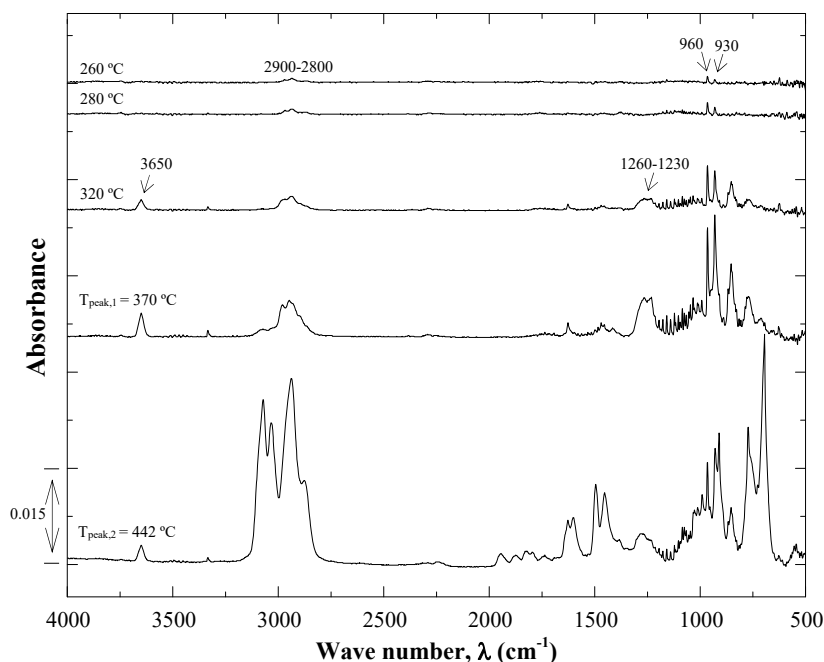


Figure 8: FT-IR spectra of ABS-APP/AlPi pyrolysis products at the temperature of the maximum mass loss rate and at the beginning of decomposition.

3.3. Flammability

The flammability behaviour (reaction to a small flame) of ABS and ABS flame retardant formulations was assessed by LOI and UL-94 vertical burning tests. The results of LOI and UL-94 tests are summarised in Table 4.

Table 4: LOI value and UL94 vertical burning tests rating for ABS and ABS flame retardant formulations.

| | ABS | ABS-APP | ABS-ALPi | ABS-APP/ALPi |
|----------------------|------|---------|----------|--------------|
| LOI | 18.0 | 23.1 | 38.1 | 29.1 |
| UL-94 classification | NC | NC | NC | V0 |

NC: *Not Classified*

It was observed that ABS cannot self-extinguish during combustion, with no rating in UL-94, and it had a LOI value of only 18%. Although, APP and ALPi got highest values of LOI, especially the ALPi which registered a LOI of 38%, they did not avoid the completely combustion of the UL-94 specimen. Only when they were together a self-extinguish behaviour was observed during the UL-94 vertical burning test. This fact indicates that, individually, the FR additives did not promote, under the UL-94 vertical burning test conditions, a flame retardant mechanism to avoid the complete combustion of the specimens. This was related with the mode of action of these FR additives. Seems that, APP produce more carbonaceous layer during combustion but was not stiff and protective enough to avoid the completely combustion. Also, ALPi which acts mainly on the gas phase, under the oxidative experimental conditions, did not effectively avoid flame propagation, probably due to an insufficient phosphorus content, unlike APP a second 10 s application was need in the case of the presence of ALPi. Although, when APP and ALPi were added to ABS, a UL V-0 classification was achieved. This was associated to the flame inhibition promoted by the liberation of phosphorus radicals during the hydrolysis of ALPi (like previously mentioned) and the formation of an effective protective layer due to the strong interactions between the PFR and the polymer, being APP the major charring promoter component [39]. It must be said that these results are coherent with other similar, where it was stated that single phosphorus-based flame retardants are unlike to give UL-94 V-0 rating for styrene plastics including ABS [8].

3.4. Forced Flaming Fire Behavior

Figure 9 presents characteristic heat release rate and total heat release curves at an external heat flux of 35 kW/m^2 and Table 5 the main results obtained from it.

As expected, ABS burned completely without significant residue formation. The HRR increased quickly after ignition, followed by a less intense increase period until reach its maximum value. This last period behaviour was related with increasing thermal feedback from the back of the sample and with the combustible consumption at the conclusion of the burning [3]. This feature indicates that the ABS combustion flame spreads rapidly, in agreement with the LOI and UL-94 results.

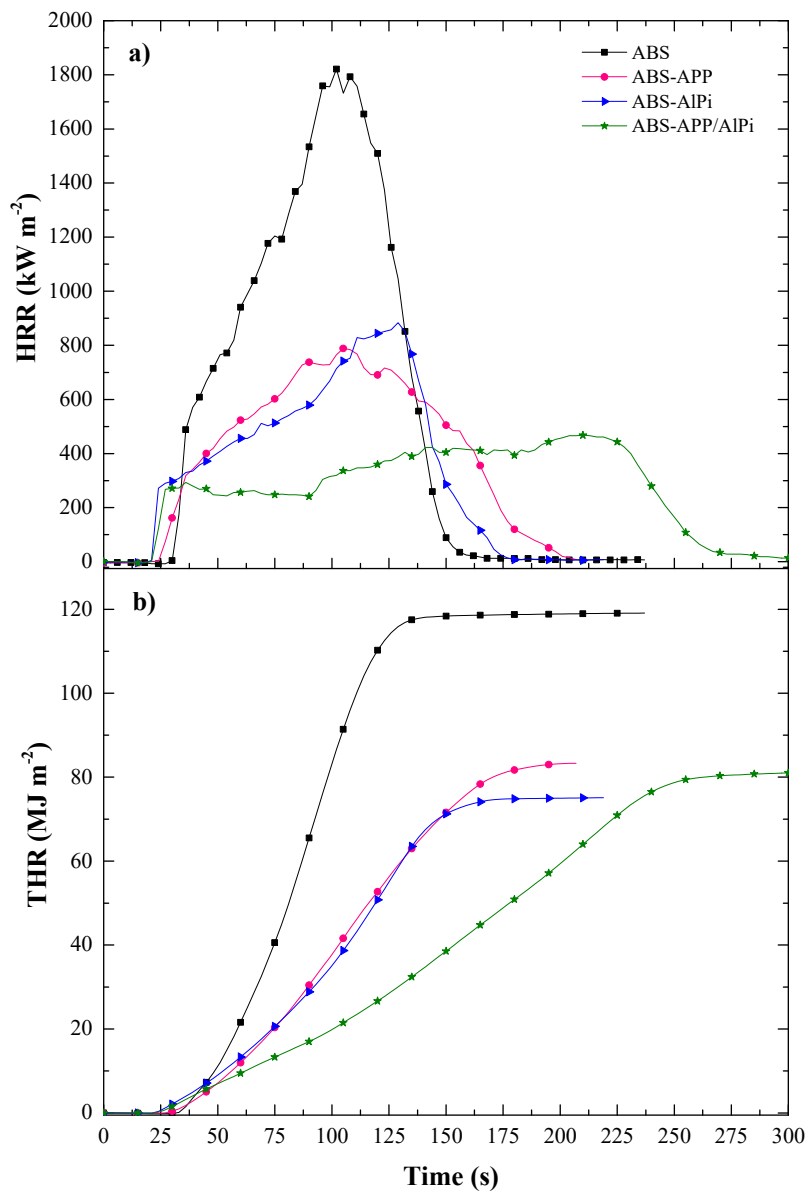


Figure 9: Heat release rate a) and total heat release b) of cone calorimeter measurements.

The ABS flame retardant systems clearly showed improvements in terms of flame retardancy, such as reduction in peak heat release rate (PHRR) and total heat evolved (THE) compared with the neat ABS. Nevertheless, all formulations showed slightly lower values of time to ignition. The ABS-AlPi curve showed an initial increase in HRR up to a shoulder, followed by a dominant peak of HRR (PHRR) at the end of burning, indicating that no efficient barrier for heat transport controlled the burning. This sample presented a residue value obtained at the end of the test of 1,7 % and the lowest value of effective heat of combustion (EHC), which indicates a flame inhibition effect as the main fire retardant mode of action, which corresponds well with the literature [14]. This result indicates the almost complete vaporization of AlPi, coherent with the pyrolysis behaviour of ABS-AlPi. By another hand, the ABS-APP showed a PHRR of 788 kW/m², slightly lower than that registered for ABS-AlPi (Figure 9 and Table 5) and a more gradual decrease of the HRR before the end of burning. This sample presented the highest value of residue (20.7 %) at the end of the combustion process and the higher EHC, which indicates that APP under forced flame flaming conditions had a prominent mode of action on the condensed phase as a residue and char promoter. It is well known that APP is able to function as flame retardant in the condensed or polymer phase through intumescence. During intumescence, a material swells when it is exposed to heat or fire to form a porous carbonaceous foam which acts as a barrier to prevent heat, air and pyrolysis product from entering the surface of the material [40].

Table 5: Main results obtained from cone calorimeter tests.

| Material code | TTI (s) | PHRR (kW m ⁻²) | t _{PHRR} (s) | MARHE (kW m ⁻²) | THE (MJ m ⁻²) | EHC (MJ kg ⁻¹) | Residue (wt%) |
|---------------|------------|-------------------------------|--------------------------|--------------------------------|------------------------------|-------------------------------|------------------|
| ABS | 30 | 1821 | 102 | 925 | 128.0 | 32.5 | 0.4 |
| ABS-APP | 26 | 788 | 104 | 487 | 83.4 | 26.6 | 20.7 |
| ABS-AlPi | 23 | 883 | 131 | 490 | 71.1 | 18.7 | 1.7 |
| ABS-APP/AlPi | 25 | 468 | 210 | 323 | 80.4 | 23.8 | 12.3 |

When both additives were present in the polymer matrix (ABS-APP/AlPi), a quasi-static plateau with a mean HRR value of approximately 230 kW/m², was observed at the beginning of the cone calorimeter measurement. This fact supports the formation of a more protective char over the sample surface during this period of time. Nevertheless, the residue content and EHC were reduced compared to the ABS-APP.

This was due to the release of phosphorus radicals during ABS-APP/AlPi decomposition, which acted like scavengers of the HO· and H· radicals, yielded during polymer combustion, and transforming its high-energy state to the steady state (coherent with the TGA-FTIR results). So, in this formulation a combination of a condensed and gas phase mode of action by the formation of a more effective protective layer and flame inhibition has occurred. This led to a more efficient flame retardant effect, consistent with the self-extinguish behaviour observed under UL-94 standard test conditions. Also, it should be mentioned that the flame retardancy efficiency of AlPi has been reported to show a nonlinear behaviour in its flame inhibition over concentration. Specifically, it was observed that its flame retardancy efficiency was levelling off for higher concentrations [12, 23]. Notwithstanding, as it was previously discussed in the TGA and FTIR analysis, the combination of APP and AlPi showed strong evidence of synergistic mechanisms, where a pseudo-synergistic effect resulted by the reduction of AlPi concentration plays no role here.

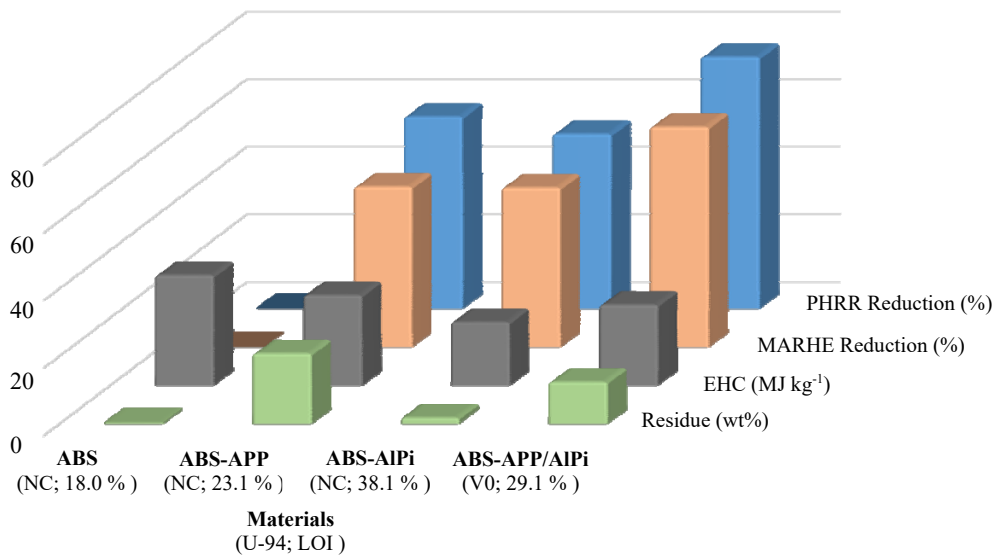


Figure 10: Comparative of the main flammability and fire behavior results of each material, obtained from UL-94, LOI and cone calorimeter tests.

On the other hand, a slow gradual increase of the HRR was observed after the mentioned stage, which indicates that the protective layer was not completely efficient by permitting subsequent heat and mass transfer until reach the PHRR. Despite that, ABS-APP/AlPi showed the highest reduction in PHRR (74%) and in MARHE index (65%) (Figure 10). It is also remarkable that, around 175 s, the ABS-APP and ABS-AlPi formulations reached their maximum THR values, while ABS-APP/AlPi had

released only a 60 % of its THE (see Figure 9 b)). Additionally, ABS-APP/AlPi arrived to the maximum THR almost 100 s latter than the other two mentioned formulations.

Also, although both ABS-APP and ABS-APP/AlPi showed an intumescent effect during the cone calorimeters experiments, the residue of ABS-APP/AlPi presented a more cohesive and uniform layer at its surface (Figure 11).



Figure 11: Photographs of the ABS flame retardant formulations residue after the cone calorimeter test.

a) ABS-APP, b) ABS-AlPi, c) ABS-APP/AlPi.

The morphology of the fire residue was also analysed on the microscopic scale to assess the quality of the protective surface layer as well as the structure formed under that surface (Figure 12). ABS-APP showed a flat surface with a poor cohesive microstructure and an under expanded layer with high size porous. Also, ABS-AlPi showed a thinner crisp layer (Figure 11) that at a microscopic level showed a cohesive smooth layer. On the other hand, when both phosphorus flame retardants were present evidences of a higher protective residue were observed. As it can be seen in Figure 12, ABS-APP/AlPi residue showed a cohesive rough surface composed by smooth particles and agglomerates of sub-micrometre high aspect-ratio particles. Also, the microstructure under that protective layer showed evidences of a crucial improvement of the protective properties of the residue. It can be seen how a foamed structure composed by closed microspheres was formed. This more effective heat insulating foamed structure combined with the cohesive upper surface layer was the key to the optimized performance on the condensed phase. This observation match well with the comparative analysis of the experimental and theoretical curves of TGA, which showed evidences of synergistic effects between APP and AlPi and related to the formation of a more thermally-stable structure.

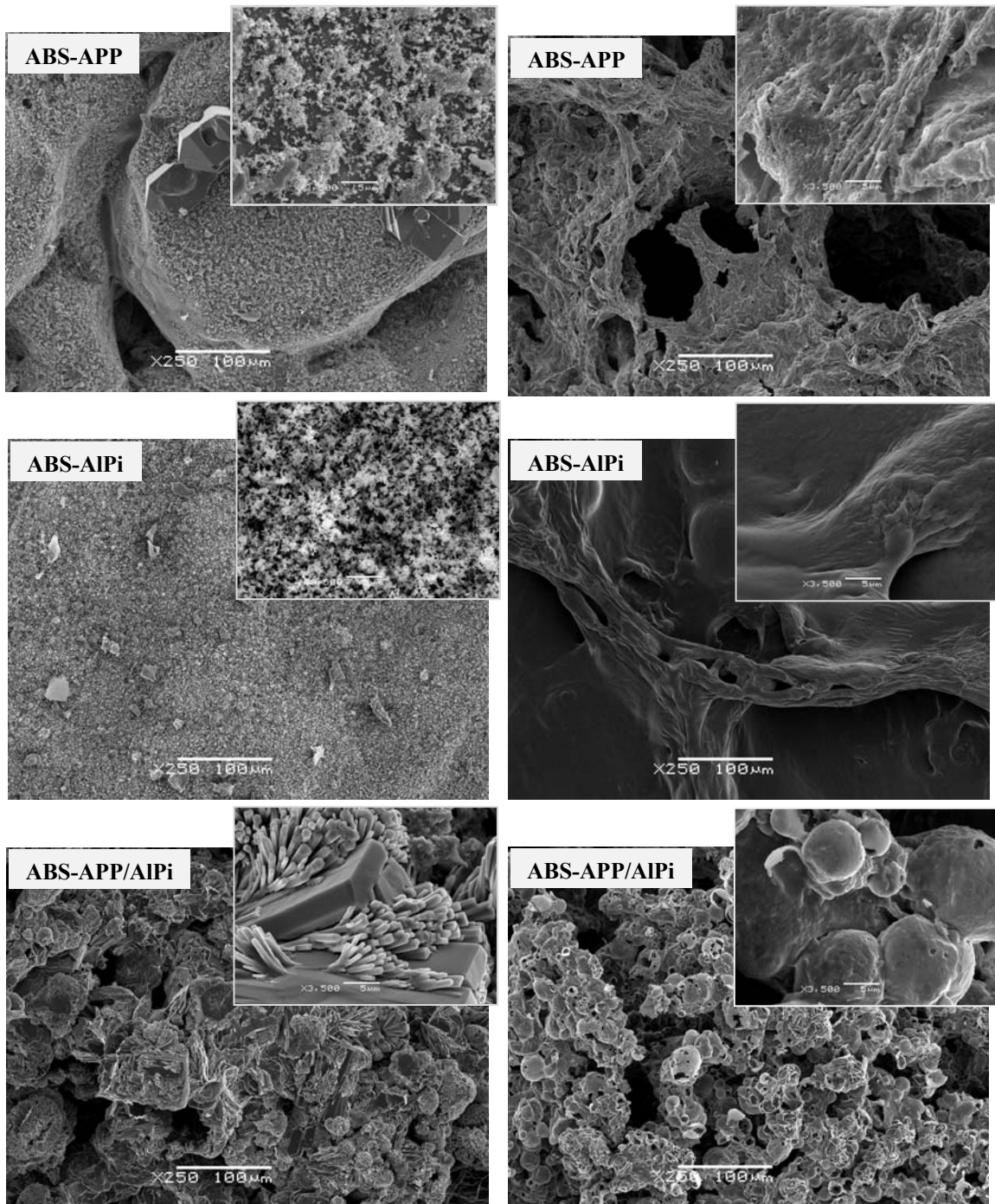


Figure 12: SEM micrographs of the upper (left) and down surface (right) of the ABS phosphorus flame retardant samples after the cone calorimeter tests (at 250 \times and 3500 \times , with a scale bar of 100 and 5 μm respectively).

Conclusions

Based on thermal decomposition, FTIR gas pyrolysis analysis, flammability and fire reaction of the ABS phosphorus flame retardant formulations, evidences of occurrence of gas-phase activity in ABS-AlPi via flame inhibition and condensed-phase activity via charring and residue formation in ABS-APP were observed.

An important flame retardancy enhancement was noted when both flame retardants were present in ABS. FTIR analysis of the pyrolysis gases revealed interactions between both additives that promoted the liberation of phosphorus radicals at a temperature range that could act like scavengers of those radicals yielded during ABS decomposition. A combined gas and condensed-phase mode of action was observed during cone calorimeter tests, that led to the higher reduction of PHRR and MARHE values, in good agreement with the TGA and gas pyrolysis FT-IR analysis as well as with the obtained V0 classification under UL-94 standard and morphology analysis of the cone calorimeter samples residue assessed by SEM.

Acknowledgements

The authors would like to acknowledge the Spanish Ministry of Economy, Industry and Competitiveness for the financial support of the projects MAT2017-89787-P and BIA2014-52688-R.

References

- [1] G.F. Giaconia, L. Castellani, C. Maestrini, T. Riccò, *Polymer*, 39 (1998) 6315-6324.
- [2] S.R. Owen, J.F. Harper, *Polym Degrad Stab*, 64 (1999) 449-455.
- [3] C.A. Wilkie, A.B. Morgan, *Fire Retardancy of Polymeric Materials*, CRC Press, 2nd Edition (2010) USA.
- [4] W.Y. Chiang, C.H. Hu, *Eur Polym J*, 35 (1999) 1295-1303.
- [5] A. Petsom, S. Roengsumran, A. Ariyaphattanakul, P. Sangvanich, *Polym Deg Stab*, 80 (2003) 17-22.
- [6] S.V. Levchik, E.D. Weil, *J Fire Sci*, 24 (2006),137-151.
- [7] M. P. Luda Di Cortemiglia MP, G. Camino G, L. Costa, *J Anal Appl Pyrol*, 11 (1987), 511-526.
- [8] S.V. Levchik, E.D. Wei, *Polym Int*, 57 (2008) 431-448.

- [9] W. Kim, D. Hoang, H. Vothi, H. C. Nguyen, T. Giang, H. An, J. Kim, *Macrom Res*, 24 (2016) 66-73.
- [10] H. Luo, F. Zhou, Y. Yang, X. Cao, X. Cai, *J Therm Anal Calorim*, 132 (2018) 263-273.
- [11] Y. Ren, Q. Fu, X. Wang, L. Yang, L. ng, J. Zhou, B. Zhong, Z. Zhang, 39 (2015) 557-569.
- [12] S. Rabe, Y. Chuenban, B. Schartel, *Materials* 10 (2017), 455
- [13] B. Schartel, B. Perret, B. Dittrich, M. Ciesielski, J. Krämer, P. Müller, V. Altstädt, L. Zang, M. Dörnig, *Macromol. Mater. Eng.* 301 (2016) 9–35
- [14] A. Sut, S. Greiser, C. Jäger, B. Schartel, *Thermochim Acta*, 640 (2016) 74–84.
- [15] F. Laoutida, L. Bonnauda, M. Alexandre, J.M. Lopez-Cuesta, Ph. Dubois, *Mater Sci Eng R Rep*, 63 (2009) 100-125.
- [16] H. Li, N. Ning, L. Zhang, Y. Wang, W. Liang, M. Tiana, *Polym Degrad and Stab*, 105 (2014) 86-95.
- [17] F. D. Sypaseuth, E. Gallo, S. Ciftci, B. Schartel, *E-Polym*, 17 (2017) 449-462.
- [18] R. Arjrandi, A. Ismail, A. Hassan, A. Bakar, *Constr Build Mater*, 152 (2017) 484-493.
- [19] Y. R. Huang, J. W. Yang, Z. Z. Wang, *J Thermplast Compos Mater*, 30 (2017) 816-826.
- [20] C. H. Ke, J. Li, K. Y. Fang, Q. L. Zhu, J. Zhu, Q. Yan, Y. Z. Wang, *Polym Degrad Stab*, 95 (2010) 763-770.
- [21] S. Sullalti, M. Colonna, C. Berti, M. Fiorini, S. Karanam, *Polym Degrad Stab*, 97 (2012), 566-572.
- [22] U. Braun, B. Schartel, M.A. Fichera, C. Jager, *Polym Degrad Stab*, 92 (2007) 1528-1545.
- [23] K. Langfeld, A. Wilke, A. Sut, S. Greiser, B. Ulmer, V. Andrievici, P. Limbach, M. Bastian, B. Schartel, *J Fire Sci*, 33 (2015),157-177.
- [24] A. Riva, G. Camino, L. Fomperie, P. Amigouet, *Polym Degrad Stab*, 82 (2003) 341-346.
- [25] Z. Wang, E. Han, W. Ke, *Prog Org Coat*, 53 (2005) 29-37.
- [26] U. Braun, B. Schartel, *Macromol Mater Eng*, 293 (2008), 206–217.
- [27] T. Orhan, N. A. Isitman, J. Hacaloglu, C. Kaynak, *Polym Degrad Stab*, 96 (2011) 1780-1787.
- [28] J. Feng, C. Carpanese, A. Fina, *Polym Degrad Stab*, 129 (2016) 319-327.

- [29] S. Bellayer, M. Jimenez, B. Prieur, B. Dewailly, A. Ramgobin, J. Sarazin, B. Revel, G. Tricot, S. Bourbigot, *Polym Degrad Stab*, 147 (2018) 159-167.
- [30] A. Castrovinci, G. Camino, C. Drevelle, S. Duquesne, C. Magniez, M. Vouters, *Eur Polym J*, 41 (2005) 2023-2033.
- [31] A. Ramani, A. E. Dahoe, *Polym Degrad. Stab*, 105 (2014) 1-11.
- [32] W. Chen, X. Fu, W. Ge, J. Xu, M. Jiang, *Polym Degrad Stab*, 102 (2014) 81–87.
- [33] S. Munteanu, C. Vasile, *J. Optoelectron. Adv. Mater.* 7 (2005) 3135-3148.
- [34] M. Suzuki, C.A. Wilkie, *Polym Degrad Stab*, 47 (1995) 217-221.
- [35] A. Riva, G. Camino, L. Fomperie, P. Amigouet, *Polym Degrad Stab*, 82 (2003) 341-346].
- [36] S. V. Levchik, G. Camino, L. Costa, G. F. Levchik, *Fire Mat* (1995) 19, 1.
- [37] S. Molyneux, A. A Stec, T. R. Hull, *Polym Degrad Stab* (2014) 36-46.
- [38] J. C. Liu, M.J. Xu, T. Lai, B. Li, *Ind Eng Chem Res*, 54 (2015) 9733-9741.
- [39] R. Sonnier, B. Otazaghine, L. Ferry, J. M. Lopez-Cuesta, *Combustion and flame* 160 (2013) 2182-2193.
- [40] K.S. Lim, S.T. Bee, L. T. Sin, T.T. Tee, C.T. Ratnam, D. Hui, A.R. Rahmat, *Comp Part B Eng*, 84 (2016) 155-174.